Ocean Sci. Discuss., 12, 2257–2281, 2015
www.ocean-sci-discuss.net/12/2257/2015/
doi:10.5194/osd-12-2257-2015

Ocean Science
Discussions
Open Access

Impact of vertical and horizontal advection on nutrient distribution in the South East Pacific

B. Barceló-Llull[1], E. Mason[2], and A. Pascual[2]

[1]Universidad de Las Palmas de Gran Canaria, ULPGC, Las Palmas de Gran Canaria, Spain
[2]Instituto Mediterráneo de Estudios Avanzados, IMEDEA (CSIC-UIB), Mallorca, Spain

Received: 13 July 2015 – Accepted: 31 August 2015 – Published: 29 September 2015

Correspondence to: B. Barceló-Llull (b.barcelo.llull@gmail.com)

Published by Copernicus Publications on behalf of the European Geosciences Union.

Abstract

An innovative approach is used to analyse the impact of vertical velocities associated with quasi-geostrophic (QG) dynamics on the distribution of a passive nutrient tracer (nitrate) in the South East Pacific. Twelve years of vertical and horizontal currents are derived from an observation-based estimate of the ocean state. Horizontal velocities are obtained through application of thermal wind balance to weekly temperature and salinity fields. Vertical velocities are estimated by integration of the QG Omega equation. Seasonal variability of the synthetic vertical velocity and kinetic energy associated with the horizontal currents are coincident, with peaks in austral summer (November–December) in accord with published observations. Two ensembles of Lagrangian particle tracking experiments that differ according to vertical forcing ($w = w_{QG}$ vs. $w = 0$) enable a quantitative analysis of the impact of the vertical velocity. From identical initial distributions of nitrate-tagged particles, the Lagrangian results show that the impact of vertical advection on nutrient distribution is 30 % of the contribution of horizontal advection. Despite being weaker by a factor of up to 10^{-4} than the horizontal currents, vertical velocity is demonstrated to make an important contribution to nutrient distributions in the region of study.

1 Introduction

Mesoscale features make an important contribution to biogeochemical cycles through the redistribution of nutrients and passive marine organisms through both horizontal advection and vertical exchange. Vertical motion plays a key role in the exchange of heat, salt and biogeochemical tracers between the surface and deep ocean. In coastal upwellings, frontal areas and mesoscale eddies, the vertical velocity has fundamental importance and can significantly contribute to nutrient supply in the euphotic zone (Mahadevan, 2014).

OSD
12, 2257–2281, 2015

Previous remote sensing studies (Chelton et al., 2011a) have revealed that chlorophyll *a* distributions within mesoscale eddies are characterized by dipole-like patterns, with extreme values found at the eddy peripheries. Chelton et al. (2011a) have proposed eddy horizontal advection to explain this distribution. On the other hand, the importance of vertical exchange for phytoplankton growth and chlorophyll *a* distribution in mesoscale oceanic eddies has been attributed to various mechanisms such as eddy pumping, eddy-induced Ekman pumping or vortex Rossby waves (McGillicuddy et al., 1998; Siegel et al., 1999; Mahadevan et al., 2012; Martin and Richards, 2001; McGillicuddy et al., 2007; Benítez-Barrios et al., 2011; Buongiorno Nardelli, 2013; Gaube et al., 2013, 2015).

In this context, we aim to quantify the importance of horizontal and vertical mesoscale motions on nutrient distribution through the application of quasi-geostrophic (QG) theory to an observation-based product (Buongiorno Nardelli et al., 2012; Pascual et al., 2015). In particular, we aim to investigate the influence of derived horizontal and vertical velocities on ocean nitrate distribution in the South East Pacific through the use of a Lagrangian particle-tracking code.

The remote South East Pacific is the least sampled oceanic region in the world ocean, in terms of both hydrography and biogeochemical structure (Ras et al., 2008). Synoptic observations from satellites provide crucial knowledge about such regions, despite their limitation to surface fields (Ducet et al., 2000; Dibarboure et al., 2011). The now mature ARGO program is a source of supplementary subsurface hydrographic data (temperature and salinity) in the form of discrete vertical profiles over a global, but sparse, grid. The ARMOR3D estimate of the ocean state (Guinehut et al., 2012) is an innovative approach where remote sensing observations (sea surface temperature and sea level anomalies) are merged with in-situ ARGO temperature and salinity profiles. The resulting multivariate observation-based dataset is freely available (see Sect. 3).

The South East Pacific has a variety of different trophic regimes (Ras et al., 2008) such as the upwelling zone near the Peru–Chile coast that is rich in nutrients and has high chlorophyll *a* concentrations, and the area associated with the central part of

OSD
12, 2257–2281, 2015

the South Pacific Gyre, which is the most oligotrophic area in the global ocean (Morel et al., 2010). Mesoscale effects on chlorophyll *a* production can be considered to differ between regions with different dynamical characteristics. Lathuiliere et al. (2011) demonstrate that, while mesoscale activity in upwelling regions leads primarily to offshore export of phytoplankton, in the oligotrophic gyres mesoscale processes promote vertical advection of nutrients into the euphotic layer, thereby stimulating primary production. The present work is focused on the same area analysed by Chelton et al. (2011a), the offshore South East Pacific (SEP, white box in Fig. 1), where nutrient input by mesoscale vertical exchange is considered to play a lead role in primary production.

Figure 1 shows the time averaged eddy kinetic energy (EKE) at the surface computed from daily AVISO (DT14, Capet et al., 2014) sea level anomalies. The EKE in the South Pacific Gyre has lower values in comparison with more active regions such as the Gulf Stream or Agulhas Current Pascual et al., 2006; Imawaki et al., 2013. However, this gyre also includes a region with relatively high EKE values corresponding to the mid-west South Pacific. Qiu and Chen (2004) and Qiu et al. (2008) attribute the high EKE values found in this region to baroclinic instability of the eastward surface Subtropical Countercurrent (STCC) and the westward South Equatorial Current (SEC). Although the SEC is a surface current near the equator, it has a subsurface component that Qiu and Chen (2004) observed as far south as 30°S, where it underlies the STCC (see Fig. 3 of Qiu and Chen, 2004). Moreover, they also find that in this region seasonal EKE modulation is related to the seasonal intensification/decay of the STCC-SEC baroclinic instability, with a maximum in November–December. In the same way, the gyre has another region with relatively high EKE values in its northwest corner. In contrast to the STCC-SEC system, Qiu and Chen (2004) attribute these high values to barotropic instabilities between the eastward South Equatorial Countercurrent (SECC) and its bordering westward SEC. The SECC-SEC system also presents seasonal EKE modulation, but with maximum in April because the SECC-SEC horizontal shear seasonality is dominated by seasonal changes in the strength of the SECC.

OSD
12, 2257–2281, 2015

The two systems analysed by Qiu and Chen (2004) additionally show interannual EKE variability.

Figure 1 shows high EKE values off the Peru–Chile coast which is characterized by an important coastal upwelling and the consequent generation of mesoscale eddies and filaments (Brown et al., 2008; Brink and Robinson, 2005; Strub et al., 2013). The region of study (white box in Fig. 1) is characterized by relatively low eddy kinetic energy, with higher EKE values in the southwest corner that are related to the STCC-SEC system, and in the eastern section, to the coastal upwelling eddy generation. However, the SEP has important eddy activity due, in part, to eddy formation in the Peru–Chile coastal upwelling (Chelton et al., 2011a).

A brief description of the synthetic temperature and salinity fields and biogeochemical data is given in Sect. 2. Section 3 describes the methodology used to diagnose the quasi-geostrophic vertical velocity, together with a description of the Lagrangian particle-tracking code utilized for the passive nutrient simulation. In Sect. 4 the results of the vertical velocity and kinetic energy analysis as well as the results of the Lagrangian simulation are discussed. Section 5 summarizes and concludes the results.

2 Data

We use the ARMOR3D observation-based product which is based on the merging of gridded satellite sea level anomaly (SLA) and sea surface temperature (SST) remote sensing observations with in-situ vertical profiles of temperature and salinity to provide a global 3-D dataset of temperature and salinity (Guinehut et al., 2012). The data are computed on a $1/3^{\circ}$ Mercator horizontal grid with weekly temporal resolution covering the period 1998–2009, with 24 vertical levels from the surface to 1500 m depth. A validation of ARMOR3D is presented by Mulet et al. (2012) who use a consistent dataset from a model reanalysis.

Auxiliary data are used to evaluate the impact of vertical and horizontal velocities on ocean nutrient distributions. Here we use climatological nitrate data from WOAPISCES

OSD
12, 2257–2281, 2015

(Penven et al., 2008). Nitrate data are chosen because their large vertical gradient over the mixed layer (Fig. 2b and 2c) highlights the contribution of vertical velocity which is characterized by smaller values than horizontal currents, but is expected to play an important role in the introduction of nutrients into the euphotic layer. Figure 2a shows the horizontal nitrate distribution at 200 m depth from WOAPISCES. High nitrate values near the Peru–Chile coast are associated with the coastal upwelling. In the zonal section (Fig. 2b) the uplift of the nitracline due to the coastal upwelling off Peru–Chile coast is most evident. In the meridional section (Fig. 2c) nitrate concentration increases northward.

3 Methodology

3.1 Computation of 3-D velocity

Horizontal velocities are computed through the geostrophic relation:

$$u_g = -\frac{1}{f}\frac{\partial \mathrm{dh}}{\partial y} \tag{1a}$$

$$v_g = +\frac{1}{f}\frac{\partial \mathrm{dh}}{\partial x} \tag{1b}$$

with the dynamic height, dh, calculated from ARMOR3D temperature and salinity profiles. f is the Coriolis parameter.

Vertical velocity is estimated using the quasi-geostrophic approximation by integrating the QG omega equation, presented here in its Q-vector formulation (Hoskins et al., 1978; Tintoré et al., 1991; Buongiorno Nardelli et al., 2012; Pascual et al., 2015):

$$N^2\nabla_h^2 w + f^2\frac{\partial^2 w}{\partial z^2} = 2\nabla\cdot\boldsymbol{Q} \tag{2a}$$

OSD
12, 2257–2281, 2015

where

$$Q = \frac{g}{\rho_0}\left(\frac{\partial \boldsymbol{v}_g}{\partial x}\cdot\nabla\rho', \frac{\partial \boldsymbol{v}_g}{\partial y}\cdot\nabla\rho'\right) \quad (2b)$$

where $\boldsymbol{v}_g$ is the geostrophic velocity vector, N the Brunt–Väisälä frequency and f the Coriolis parameter. In this implementation, N only depends on depth. The Rossby number for mesoscale eddies in the SEP is generally less than 0.1 (Chelton et al., 2011b), hence we assume QG theory to be a good approximation for computing the vertical velocity in this region.

Following Eq. (2), vertical velocity is estimated from density stratification and the geostrophic velocity field. The computational code is derived following the QG vorticity and thermodynamic equations (Buongiorno Nardelli et al., 2012). Boundary conditions are constructed by considering zero vertical velocity at the upper, lower and lateral boundaries.

A sensitivity analysis was carried out in order to evaluate the influence of reference level choice on the vertical velocity estimation. The choice of reference level is influential over the first hundred meters above the bottom due to the imposed boundary condition; away from the bottom the same patterns were seen for different choices of reference level (500 and 1000 m). Testing the 500 m reference level, the vertical velocity patterns pointed to a maximum decrease in magnitude of 50 %. Hence, a reference level of 1000 m depth was chosen. Dirichlet and Neumann conditions at the lateral boundaries were tested for which we found no significant impacts on results a few points away from the boundaries.

3.2 Lagrangian simulations

In order to analyze the respective contributions of the horizontal and vertical velocity components on the distribution of a limiting nutrient, a Lagrangian particle-tracking code is used to simulate water parcel trajectories forced by the derived ARMOR3D

OSD
12, 2257–2281, 2015

velocity fields. The tracking code is ROMS Offline (Roff, e.g. Capet et al., 2008; Carr et al., 2008; Mason et al., 2012). Two sets of 30 day simulations were carried out for each week of 2009: the first set was forced with geostrophic horizontal velocity and QG vertical velocity (UVW); for the second set the same geostrophic horizontal velocity was applied but vertical velocity was set to zero (UV). Each experiment was initialised with 40 000 floats placed randomly between 150–250 m depth within the study region (white box in Fig. 2). Float positions were stored every day as output of the Lagrangian simulation. Each water parcel is tagged with the nearest value from the WOAPISCES nitrate database. This nitrate concentration value is considered a passive tracer and therefore remains unchanged with time such that we can evaluate its evolving distribution within the domain.

4 Results

4.1 QG vertical velocity and kinetic energy from observation-based product

A comparison between vertical velocity, w, and kinetic energy (KE) computed from the ARMOR3D derived geostrophic velocities is carried out in order to evaluate their relationship. An energetic region with high vertical velocities and mesoscale eddy activity is located in the southwest of the SEP, in both the vertical velocity (Fig. 3a) and kinetic energy (Fig. 3c) maps. This high eddy energy is related to baroclinic instabilities associated with the eastward surface Subtropical Countercurrent (STCC) and the westward underlying South Equatorial Current (SEC) system (Qiu and Chen, 2004; Qiu et al., 2008). Figure 3c shows other regions with elevated mesoscale activity that is associated with less intense vertical velocity values. These regions are the coastal upwelling and the SECC-SEC system explained in Sect. 1.

Vertical velocity in the energetic region in the southwest is highlighted in the zoom in Fig. 3b. Intense vertical motions of order 2–3 m day^{-1} with alternating signs are located along meanders and inside eddies. The mesoscale eddies are characterized by

OSD
12, 2257–2281, 2015

dipole-like patterns with upwelling and downwelling cells at the eddy peripheries (e.g., 126–128° W and 23–25° S). Vertical velocity around anticyclonic meanders (e.g., 136–139° W and 24–26° S or 120–122° W and 24–26° S) shows the expected upwellings in the upstream and downwellings in the downstream portions of the meander crests (Pollard and Regier, 1992; Pascual et al., 2015). Similarly, downwellings and upwellings in cyclonic meanders (e.g., 137–140° W and 24.5–26° S) are located upstream and downstream of the crest, respectively.

In order to analyse the variability of w, the standard deviation over the period 7 January 1998 to 30 December 2009 is computed and shown in Fig. 4a. In the same way, Fig. 4b shows the standard deviation of the KE. The active region in the southwest of the SEP also presents high temporal variability in both fields. The correlation coefficient between both fields in this region reaches 0.85. Considering the whole area of study the correlation coefficient is 0.79. It should be noted that this high correlation between the two variables could not be anticipated a priori as the relationship is not linear (see Eq. 2). Further, this result does not give any indication of the sign of the vertical motion, only its magnitude.

Time series of spatial averages of vertical velocity magnitude and kinetic energy are shown in Fig. 5. There is clear seasonal variability in both variables, with maximums in austral summer and minimums in austral winter related to the seasonal intensification/decay of the STCC-SEC vertical shear and, in consequence, with the increase/decrease of baroclinic instability (Qiu et al., 2008). Interannual variability and weak variability of high frequency are also shown in these figures. When averaging over only the highly energetic region in the southwest (not shown) the tendency is similar but the magnitude is double.

4.2 Lagrangian simulations

Figure 6a shows the initial positions of water parcels located between 190 and 210 m depth, and their associated passive trace nitrate values. The same water parcels are advected for both the UV and UVW simulations in order to properly compare the two

OSD
12, 2257–2281, 2015

cases (see Fig. 7a). After 30 days of simulation, the water parcels are located in new positions due to the corresponding velocity forcing (Figs. 6b and 7b). The initial (not shown) and advected (Figs. 6c and 7c) nitrate fields are obtained by bin averaging the nitrate tagged water parcels over a $0.5^\circ \times 0.5^\circ$ grid at the beginning and end of the respective simulations.

Figures 6c and 7c illustrate how the initially smooth nitrate field is modified by (i) the horizontal velocity (UV simulation) and (ii) the total velocity (UVW simulation) fields, respectively. Small scale structures are formed during the 30 days of simulation, with small differences arising as a result of the vertical velocity contribution. To better see these differences and to quantify the influence of horizontal and vertical motions in the Lagrangian simulations separately, anomalies are computed (see Eq. 3). For the UV simulation, subtracting the initial nitrate field from the final nitrate field gives an indication of the contribution of the horizontal velocity to the final nitrate distribution, i.e., the anomaly aUV (Fig. 8b). In the same way, the anomaly aUVW (Fig. 8a) gives an indication of the contribution of the total velocity. By subtracting the horizontal anomaly aUV from the total anomaly aUVW, the contribution of the vertical velocities, i.e., the anomaly aW can be isolated (Fig. 8c).

$$\mathrm{aUV} = \mathrm{UV}(t_{\mathrm{end}}) - \mathrm{UV}(t_{\mathrm{ini}}), \tag{3a}$$

$$\mathrm{aUVW} = \mathrm{UVW}(t_{\mathrm{end}}) - \mathrm{UVW}(t_{\mathrm{ini}}), \tag{3b}$$

$$\mathrm{aW} = \mathrm{aUVW} - \mathrm{aUV} \tag{3c}$$

Figure 8a and 8b presents small differences because of the vertical velocity contribution which are highlighted in Fig. 8c. Although the anomalies due to vertical velocitiy are smaller than aUV and aUVW, they are not negligible. The vertical velocity has the highest contribution off coastal upwelling zone because the moderate vertical velocity values characteristic of the eastern part of the SEP act on an important vertical nitrate gradient (see Fig. 2b) caused by the uplift of the nitracline due to the coastal upwelling. On the other hand, on the southwestern part of the SEP, characterized by higher dynamic activity, vertical velocity has low contribution due to the deeper nitracline.

OSD
12, 2257–2281, 2015

The same procedure is performed for a total ensemble of 10 simulations in order to obtain robust results. The 30 day simulations are initialized over consecutive weeks: 31 December 2008, 7 January 2009, 14 January 2009, etc. Table 1 shows the root mean square of aUV ($rmsN_H$) and aW ($rmsN_V$). This statistical parameter provides a measure of the variability in the anomaly fields. The variability of the anomaly explained by the horizontal velocity has values ranging from 0.849 to 1.007 µmol L^{-1}, i.e., the $rmsN_H$ range of values is consistent in all simulations. The variability of aW is approximately 0.3 µmol L^{-1} in all simulations. We can therefore assume that the vertical velocity explains approximately 30 % of the nitrate distributions observed in our experiments.

5 Discussion and conclusions

This paper analyses vertical velocities associated with QG dynamics as derived through an innovative approach that uses the ARMOR3D global observation-based product. Weekly horizontal geostrophic velocity and QG vertical velocity are computed from ARMOR3D temperature and salinity in the South East Pacific. Two groups of Lagrangian simulations are forced with these 3-D velocity fields. One group of simulations uses the 3-D geostrophic velocities and QG vertical velocity in order to evaluate their combined contribution to nitrate distribution. The second group of simulations is forced with 3-D geostrophic velocities with zero vertical velocity in order to evaluate the horizontal velocity contribution to the nitrate distribution. With these respective contributions, we isolate the QG vertical velocity contribution to nitrate distribution. With the root mean square statistical parameter, we obtain an estimate of nitrate distribution variability that can be explained by QG vertical velocity. In comparison with the horizontal velocity contribution, the vertical velocity explains about 30 % of the nitrate distribution. In support of this result, a sensitivity analysis produced similar values. Although we only analyse the mesoscale vertical velocity, the importance of submesoscale features on vertical tracer dispersion has been shown by (Klein and Lapeyre, 2009). Because

OSD
12, 2257–2281, 2015

of this, the vertical velocity contribution estimated here can be considered an underestimation of the real vertical velocity contribution. Fine resolution satellite observations can help to better evaluate the impact of vertical motion on nutrient distribution. The wide-swath SWOT altimeter will allow unique observations in the 15–100 km range of wavelength scales when it comes online in the next decade (Fu and Ferrari, 2008).

We have also analysed the QG vertical velocity in order to understand its distribution. The southwest of the SEP has relatively high mesoscale activity with vertical velocities exceeding 2 m day^{-1}, which is on the order of 10^{-4} times the horizontal velocity. Despite its relatively small magnitude, the vertical velocity makes an important contribution to marine ecosystem growth through the introduction of nutrients into the euphotic layer. This is demonstrated by our analysis since the most important contribution of the vertical velocity on nitrate distribution is seen to be localized to the eastern part of the SEP which is characterized by moderate vertical velocity values and a high vertical nitrate gradient.

An additional result obtained from the QG vertical velocity and kinetic energy analysis is that vertical velocity and kinetic energy have similar and intense seasonal variability with maximums in austral summer (November–December), which suggests that these quantities are mostly influenced by the seasonal modulation of STCC-SEC vertical shear (Qiu and Chen, 2004; Qiu et al., 2008).

Acknowledgements. This work has been carried out as part of E-MOTION (CTM2012-31014) project funded by the Spanish National Research Program. Additional funding from the Local Government of the Balearic Islands (CAIB-51/2011 grant) is also acknowledged. Bàrbara Barceló-Llull is supported by a pre-doctoral grant from the Spanish National Research Program associated to the PUMP (CTM2012-33355) project. Evan Mason is supported by a post-doctoral grant from the Conselleria d'Educació, Cultura i Universitats del Govern de les Illes Balears (Mallorca, Spain) and the European Social Fund. The ARMOR3D dataset was produced by CLS with support from MyOcean project (EU no. FP7-SPACE-2007-1-Grant Agreement 218812). Nitrate data were extracted from the WOAPISCES biogeochemical climatology.

OSD
12, 2257–2281, 2015

References

Benítez-Barrios, V., Pelegrí, J. L., Hernández-Guerra, A., Lwiza, K. M. M., Gomis, D., Vélez-Belchí, P., and Hernández-León, S.: Three-dimensional circulation in the NW Africa coastal transition zone, Prog. Oceanogr., 91, 516–533, doi:10.1016/j.pocean.2011.07.022, 2011. 2259

Brink, K. H. and Robinson, A. R. (Eds.): The Sea, Vol. 11: The Global Coastal Ocean: Regional Studies and Syntheses, Harvard University Press, Cambridge, MA, 2005. 2261

Brown, S. L., Landry, M. R., Selph, K. E., Jin Yang, E., Rii, Y. M., and Bidigare, R. R.: Diatoms in the desert: plankton community response to a mesoscale eddy in the subtropical North Pacific, Deep-Sea Res., 55, 1321–1333, doi:10.1016/j.dsr2.2008.02.012, 2008. 2261

Buongiorno Nardelli, B.: Vortex waves and vertical motion in a mesoscale cyclonic eddy, J. Geophys. Res.-Oceans, 118, 5609–5624, 2013. 2259

Buongiorno Nardelli, B., Guinehut, S., Pascual, A., Drillet, Y., Ruiz, S., and Mulet, S.: Towards high resolution mapping of 3-D mesoscale dynamics from observations, Ocean Sci., 8, 885–901, doi:10.5194/os-8-885-2012, 2012. 2259, 2262, 2263

Capet, A., Mason, E., Rossi, V., Troupin, C., Faugère, Y., Pujol, I., and Pascual, A.: Implications of refined altimetry on estimates of mesoscale activity and eddy-driven offshore transport in the Eastern Boundary Upwelling Systems, Geophys. Res. Lett., 41, 7602–7610, doi:10.1002/2014GL061770, 2014. 2260, 2274

Capet, X. J., Campos, E. J., and Paiva, A. M.: Submesoscale activity over the Argentinian shelf, Geophys. Res. Lett., 35, L15605, doi:10.1029/2008GL034736, 2008. 2264

Carr, S. D., Capet, X. J., McWilliams, J. C., Pennington, J. T., and Chavez, F. P.: The influence of diel vertical migration on zooplankton transport and recruitment in an upwelling region: estimates from a coupled behavioral-physical model, Fish. Oceanogr., 17, 1–15, doi:10.1111/j.1365-2419.2007.00447.x, 2008. 2264

Chelton, D. B., Gaube, P., Schlax, M. G., Early, J. J., and Samelson, R. M.: The influence of nonlinear mesoscale eddies on near-surface oceanic chlorophyll, Science, 334, 328–332, 2011a. 2259, 2260, 2261

Chelton, D. B., Schlax, M. A., and Samelson, R. M.: Global observations of nonlinear mesoscale eddies, Prog. Oceanogr., 91, 167–216, doi:10.1016/j.pocean.2011.01.002, 2011b. 2263

OSD
12, 2257–2281, 2015

Dibarboure, G., Pujol, M.-I.., Briol, F., Le Traon, P.-Y., Larnicol, G., Picot, N., Mertz, F., and Ablain, M.: Jason-2 in DUACS: updated system description, first tandem results and impact on processing and products, Mar. Geod., 34, 214–241, 2011. 2259

Ducet, N., Le Traon, P.-Y., and Reverdin, G.: Global high-resolution mapping of ocean circulation from TOPEX/Poseidon and ERS-1 and -2, J. Geophys. Res., 105, 19477–19498, 2000. 2259

Fu, L.-L. and Ferrari, R.: Observing oceanic submesoscale processes from space, EOS T. Am. Geophys. Un., 89, 488–488, 2008. 2268

Gaube, P., Chelton, D. B., Strutton, P. G., and Behrenfeld, M. J.: Satellite observations of chlorophyll, phytoplankton biomass, and Ekman pumping in nonlinear mesoscale eddies, J. Geophys. Res., 118, 6349–6370, 2013. 2259

Gaube, P., Chelton, D. B., Samelson, R. M., Schlax, M. G., and O'Neill, L. W.: Satellite observations of mesoscale eddy-induced Ekman pumping, J. Phys. Oceanogr., 45, 104–132, doi:10.1175/JPO-D-14-0032.1, 2015. 2259

Guinehut, S., Dhomps, A.-L., Larnicol, G., and Le Traon, P.-Y.: High resolution 3-D temperature and salinity fields derived from in situ and satellite observations, Ocean Sci., 8, 845–857, doi:10.5194/os-8-845-2012, 2012. 2259, 2261

Hoskins, B. J., Draghici, I., and Davies, H. C.: A new look at the ω-equation, Q. J. Roy. Meteor. Soc., 104, 31–38, 1978. 2262

Imawaki, S., Bower, A. S., Beal, L., and Qiu, B.: Western boundary currents, chapt. 13, in: Ocean Circulation and Climate – a 21st Century Perspective, edited by: Siedler, G., Griffies, S. M., Gould, J., and Church, J. A., vol. 103 of International Geophysics, Academic Press, Oxford, Amsterdam, doi:10.1016/B978-0-12-391851-2.00013-1, 305–338, 2013. 2260

Klein, P. and Lapeyre, G.: The oceanic vertical pump induced by mesoscale and submesoscale turbulence, Annu. Rev. Marine Sci., 1, 351–375, doi:10.1146/annurev.marine.010908.163704, 2009. 2267

Lathuiliere, C., Levy, M., and Echevin, V.: Impact of eddy-driven vertical fluxes on phytoplankton abundance in the euphotic layer, J. Plankton Res., 33, 827–831, 2011. 2260

Mahadevan, A.: Eddy effects on biogeochemistry, Nature, 506, 168–169, 2014. 2258

Mahadevan, A., D'Asaro, E., Lee, C., and Perry, M. J.: Eddy-driven stratification initiates North Atlantic spring phytoplankton blooms, Science, 336, 54–58, 2012. 2259

Martin, A. P. and Richards, K. J.: Mechanisms for vertical nutrient transport within a North Atlantic mesoscale eddy, Deep-Sea Res. Pt. II, 48, 757–773, 2001. 2259

OSD
12, 2257–2281, 2015

Mason, E., Colas, F., and Pelegrí, J. L.: A Lagrangian study tracing water parcel origins in the Canary Upwelling System, Sci. Mar., 76, 79–94, doi:10.3989/scimar.03608.18D, 2012. 2264
McGillicuddy, D. J., Robinson, A. R., Siegel, D. A., Jannasch, H. W., Johnson, R., Dickey, T. D., McNeil, J., Michaels, A. F., and Knap, A. H.: Influence of mesoscale eddies on new production in the Sargasso Sea, Nature, 394, 263–266, 1998. 2259
McGillicuddy, D. J., Anderson, L. A., Bates, N. R., Bibby, T., Buesseler, K. O., Carlson, C. A., Davis, C. S., Ewart, C., Falkowski, P. G., Goldthwait, S. A., Hansell, D. A., Jenkins, W. J., Johnson, R., Kosnyrev, V. K., Ledwell, J. R., Li, Q. P., Siegel, D. A., and Steinberg, D. K.: Eddy wind interactions stimulate extraordinary mid-ocean plankton blooms, Science, 316, 1021–1026, 2007. 2259
Morel, A., Claustre, H., and Gentili, B.: The most oligotrophic subtropical zones of the global ocean: similarities and differences in terms of chlorophyll and yellow substance, Biogeosciences, 7, 3139–3151, doi:10.5194/bg-7-3139-2010, 2010. 2260
Mulet, S., Rio, M.-H., Mignot, A., Guinehut, S., and Morrow, R.: A new estimate of the global 3-D geostrophic ocean circulation based on satellite data and in-situ measurements, Deep-Sea Res. Pt. II, 77–80, 70–81, 2012. 2261
Pascual, A., Faugère, Y., Larnicol, G., and Le Traon, P.-Y.: Improved description of the ocean mesoscale variability by combining four satellite altimeters, Geophys. Res. Lett., 33, L02611, doi:10.1029/2005GL024633, 2006. 2260
Pascual, A., Ruiz, S., Buongiorno Nardelli, B., Guinehut, S., Iudicone, D., and Tintoré, J.: Net primary production in the Gulf Stream sustained by quasi-geostrophic vertical exchanges, Geophys. Res. Lett., 42, 441–449, doi:10.1002/2014GL062569, 2015. 2259, 2262, 2265
Penven, P., Marchesiello, P., Debreu, L., and Lefèvre, J.: Software tools for pre- and post-processing of oceanic regional simulations, Environ. Modell. Softw., 23, 660–662, 2008. 2262
Pollard, R. T. and Regier, L. A.: Vorticity and vertical circulation at an Ocean front, J. Phys. Oceanogr., 22, 609–625, doi:10.1175/1520-0485(1992)022<0609:VAVCAA>2.0.CO;2, 1992. 2265
Qiu, B. and Chen, S.: Seasonal modulations in the eddy field of the South Pacific Ocean, J. Phys. Oceanogr., 34, 1515–1527, doi:10.1175/1520-0485(2004)034<1515:SMITEF>2.0.CO;2, 2004. 2260, 2261, 2264, 2268, 2274
Qiu, B., Scott, R. B., and Chen, S.: Length scales of eddy generation and nonlinear evolution of the seasonally modulated South Pacific Subtropical Countercurrent, J. Phys. Oceanogr., 38, 1515–1528, 2008. 2260, 2264, 2265, 2268

OSD
12, 2257–2281, 2015

Ras, J., Claustre, H., and Uitz, J.: Spatial variability of phytoplankton pigment distributions in the Subtropical South Pacific Ocean: comparison between in situ and predicted data, Biogeosciences, 5, 353–369, doi:10.5194/bg-5-353-2008, 2008. 2259

Siegel, D. A., McGillicuddy Jr., D. J., and Fields, E. A.: Mesoscale eddies, satellite altimetry, and new production in the Sargasso Sea, J. Geophys. Res.-Oceans, 104, 13359–13379, 1999. 2259

Strub, P. T., Combes, V., Shillington, F. A., and Pizarro, O.: Currents and processes along the eastern boundaries, chapt. 14, in: Ocean Circulation and Climate – a 21st Century Perspective, edited by: Siedler, G., Griffies, S. M., Gould, J., and Church, J. A., vol. 103 of International Geophysics, Academic Press, Oxford, Amsterdam, doi:10.1016/B978-0-12-391851-2.00014-3, 339–384, 2013. 2261

Tintoré, J., Gomis, D., Alonso, S., and Parrilla, G.: Mesoscale dynamics and vertical motion in the Alborán Sea, J. Phys. Oceanogr., 21, 811–823, doi:10.1175/1520-0485(1991)021<0811:MDAVMI>2.0.CO;2, 1991. 2262

OSD
12, 2257–2281, 2015

Table 1. Root mean squares of aUV ($rmsN_H$) and aW ($rmsN_V$) from the Lagrangian experiments.

Simulation	$rmsN_H$ [$\mu mol\,L^{-1}$]	$rmsN_V$ [$\mu mol\,L^{-1}$]
31 Dec 2008	0.851	0.321
7 Jan 2009	0.849	0.341
14 Jan 2009	0.884	0.345
21 Jan 2009	0.900	0.322
28 Jan 2009	0.912	0.338
4 Feb 2009	0.952	0.311
11 Feb 2009	1.007	0.370
18 Feb 2009	1.007	0.315
25 Feb 2009	0.971	0.302
4 Mar 2009	0.959	0.380

OSD
12, 2257–2281, 2015

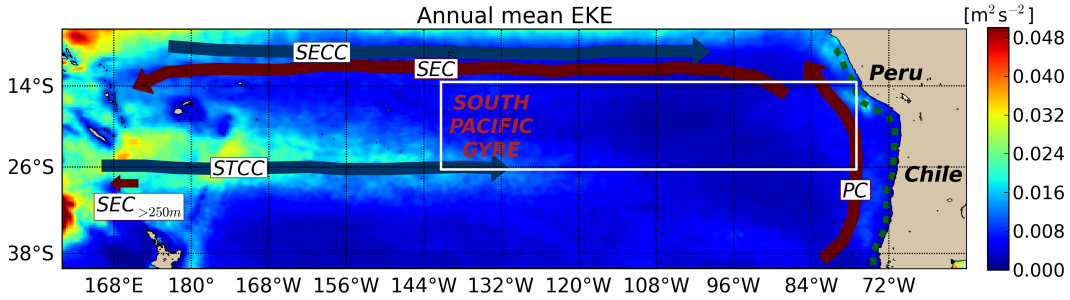

Figure 1. Map of the South East Pacific. Colours show annual mean eddy kinetic energy (EKE) computed from daily AVISO (DT14, Capet et al. (2014)) sea level anomaly data for the period 1993–2013. The white box shows the limits of the area of study. Key: SEC, South Equatorial Current; SECC, South Equatorial Countercurrent; STCC, Subtropical Countercurrent; PC, Peru Current. Green dashed line is the coastal upwelling. The small arrow indicates the poleward extent of the subsurface component of the SEC as observed by Qiu and Chen (2004) between 12–30° S at 170° E.

OSD
12, 2257–2281, 2015

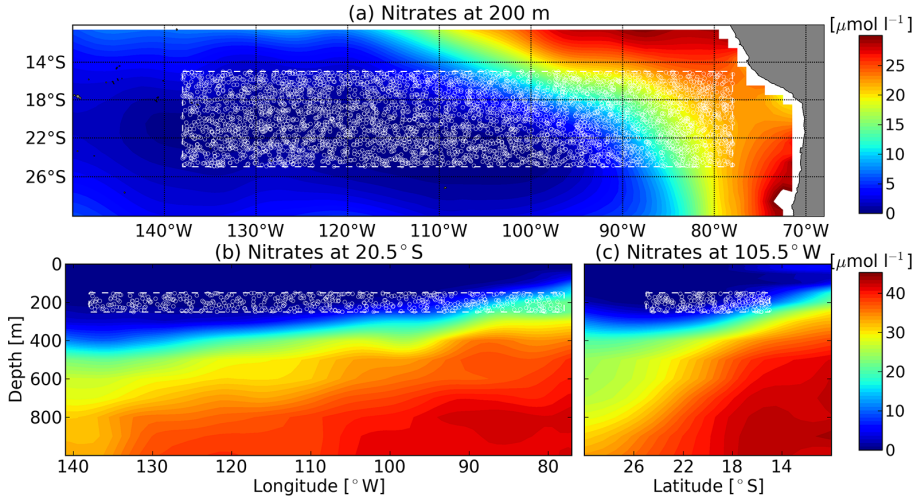

Figure 2. Climatological January mean nitrate from WOAPISCES in the South East Pacific. **(a)** Horizontal section at 200 m depth, **(b)** vertical section at 20.5° S, and **(c)** vertical section at 105.5° W. Discontinuous white lines delimit the Lagrangian simulation particle release area. White dots are a random sample of the simulated water parcels at their initial positions.

OSD
12, 2257–2281, 2015

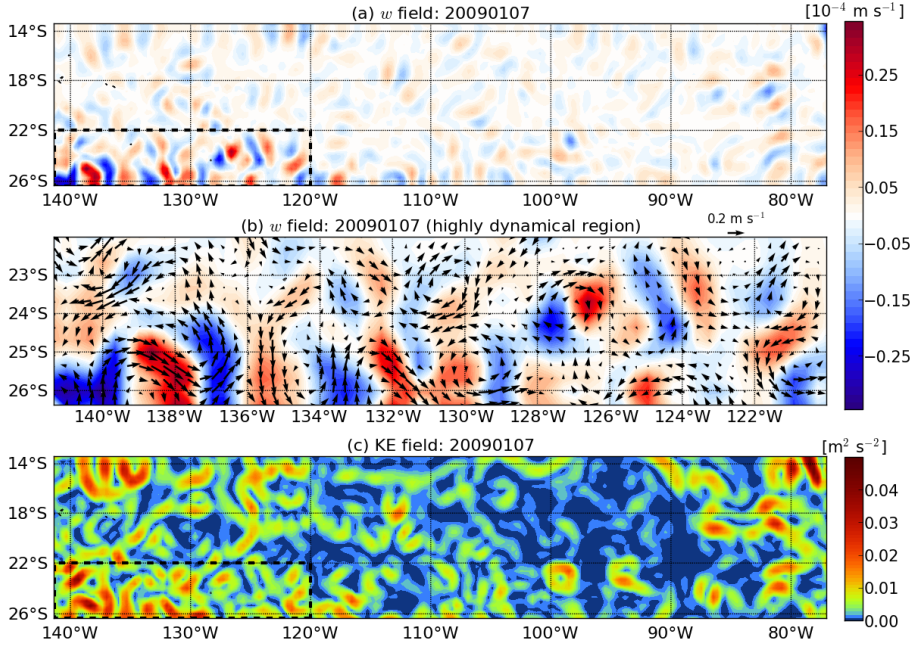

Figure 3. (a) Vertical velocity on 7 January 2009 at 200 m depth. Black box delimits the region of high mesoscale eddy activity. **(b)** Zoom of vertical velocity and horizontal geostrophic currents over the high mesoscale eddy activity region in **(a)**. **(c)** Kinetic energy on 7 January 2009 at 200 m depth.

OSD
12, 2257–2281, 2015

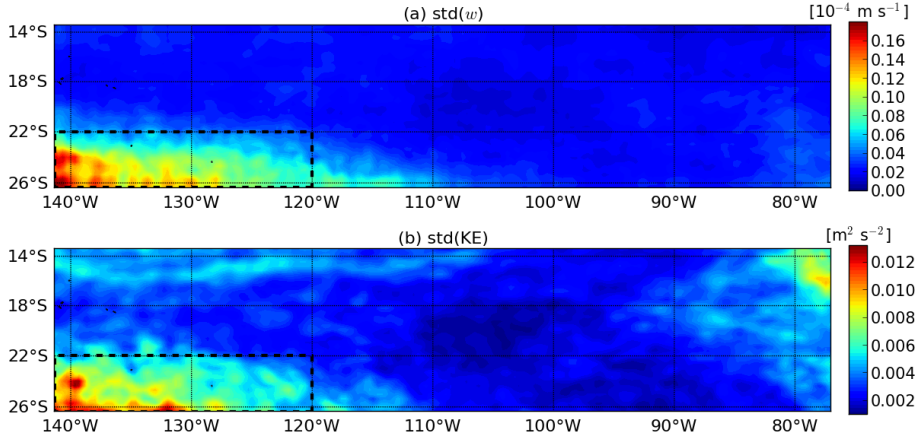

Figure 4. (a) Standard deviation of vertical velocity and **(b)** kinetic energy over the period 7 January 1998 to 30 December 2009 at 200 m depth. The discontinuous line delimits the region of high mesoscale variability.

OSD
12, 2257–2281, 2015

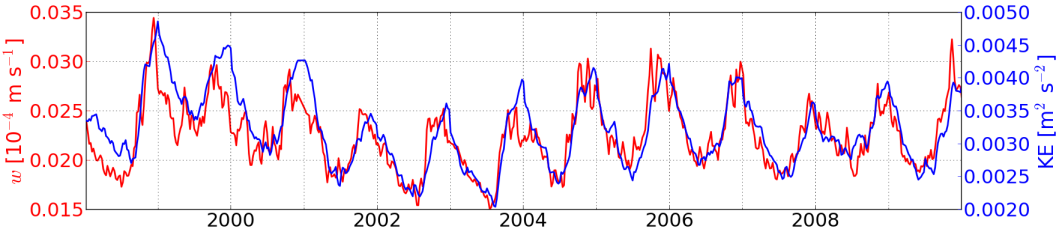

Figure 5. Time series of vertical velocity magnitude (red line) and kinetic energy (blue line) averaged over the area of study. The correlation coefficient between vertical velocity and kinetic energy is 0.84.

OSD
12, 2257–2281, 2015

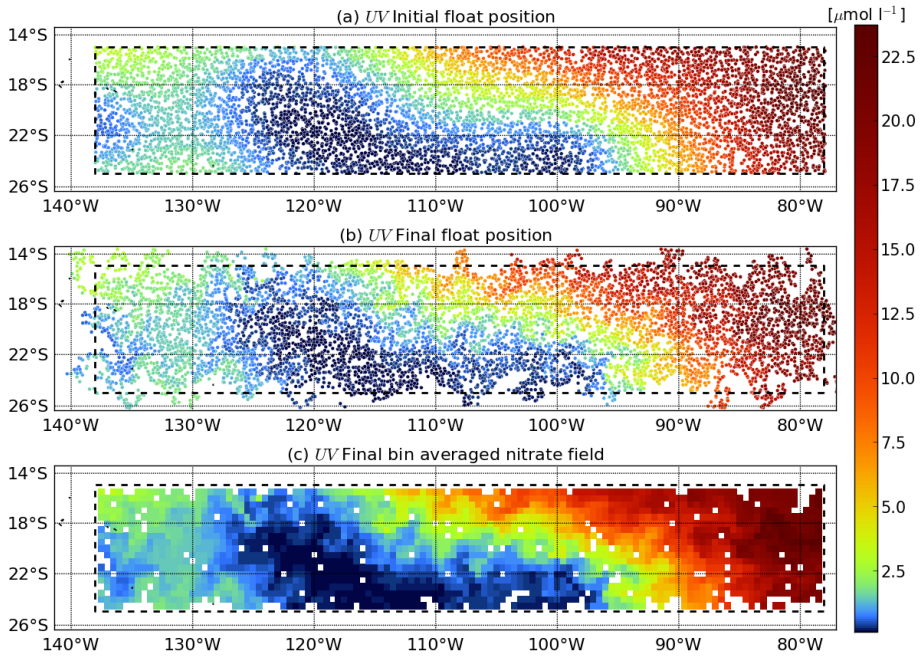

Figure 6. UV simulation (31 December 2008). **(a)** Initial positions of water parcels between 190 and 210 m depth and associated nitrate concentrations. **(b)** Positions of water particles between 190 and 210 m depth and associated nitrate concentrations after 30 days of forcing by geostrophic horizontal velocity and zero vertical velocity. **(c)** Final nitrate field computed by bin averaging the nitrate tagged fluid parcels over a 0.5° × 0.5° grid after 30 days of simulation. Black box delimits the analysed area.

OSD
12, 2257–2281, 2015

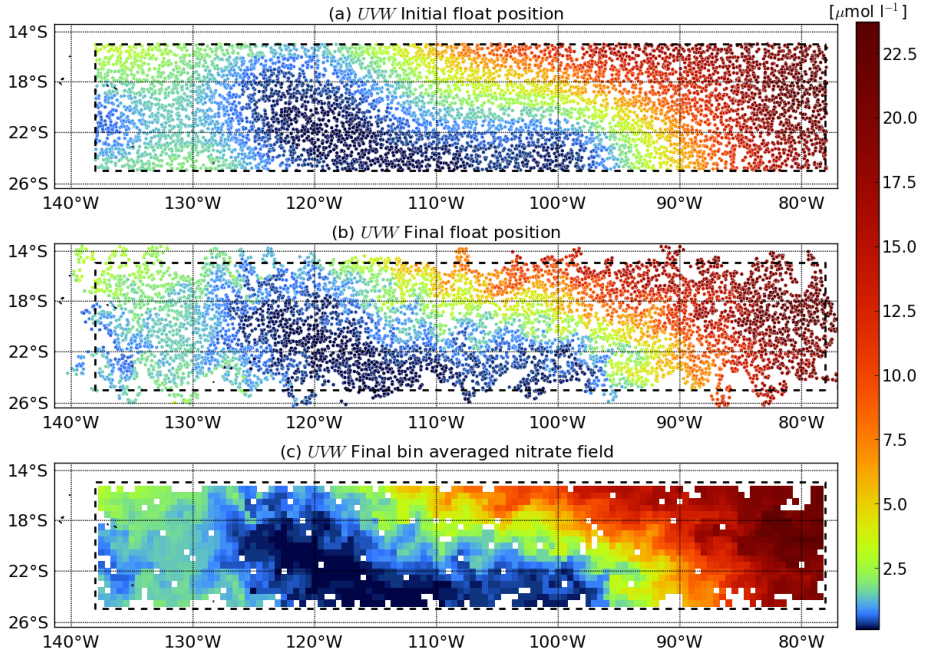

Figure 7. UVW simulation (31 December 2008). **(a)** Initial positions of water parcels between 190 and 210 m depth and associated nitrate concentrations. **(b)** Positions of water particles between 190 and 210 m depth and associated nitrate concentrations after 30 days of forcing by geostrophic horizontal velocity and QG vertical velocity. **(c)** Final nitrate field computed by bin averaging the nitrate tagged fluid parcels located over a $0.5^{\circ} \times 0.5^{\circ}$ grid after 30 days of simulation. Black box delimits the analysed area.

OSD
12, 2257–2281, 2015

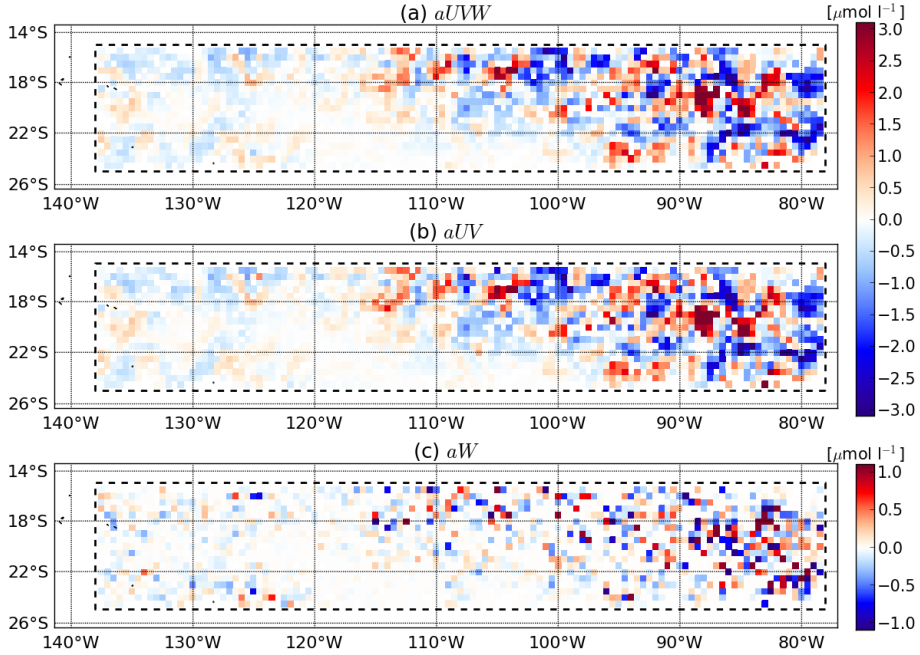

Figure 8. (31 December 2008 simulation) Nitrate anomalies resulting from **(a)** contributions from both QG vertical velocity and geostrophic horizontal velocity (aUVW); **(b)** the contribution from only geostrophic horizontal velocity (aUV); and **(c)** the QG vertical velocity contribution (aW).

OSD
12, 2257–2281, 2015